

---

---

STRUCTURE, PHASE TRANSFORMATIONS,  
AND DIFFUSION

---

---

## Effect of Sol-Gel Sealing Method on the Corrosion Resistance of Plasma-Sprayed WC–12% Co Coatings

M. A. Ashraf<sup>a</sup>, A. Salman<sup>a</sup>, M. U. Manzoor<sup>a</sup>, \*, and A. Farooq<sup>a</sup>

<sup>a</sup> Institute of Metallurgy & Materials Engineering, University of the Punjab, Lahore, 54590 Pakistan

\*e-mail: umar.imme@pu.edu.pk

Received March 11, 2021; revised May 12, 2021; accepted May 20, 2021

**Abstract**—Plasma sprayed WC–12% Co coatings have been used in various engineering applications such as wear-resistant nozzles, cutting tools, and drill bits due to their excellent mechanical properties. However, the corrosion properties of these coatings leave much to be desired because of the higher percentage of porosity, which allows the corrosive media to travel through the coating surface and reach the metallic substrate. This work is aimed at sealing the pores in plasma-sprayed WC–12% Co coatings by the sol-gel method to increase their corrosion resistance. The percentage of porosity in the as-sprayed and sealed coatings was estimated by the ASTM standard method. Moreover, the presence of sealant in the pores was confirmed by scanning electron microscopy (SEM) and the energy-dispersive X-ray spectroscopy (EDS) analysis. The electrochemical tests were employed to study the corrosion resistance of as-sprayed and sealed coatings in 3.5 wt % NaCl solution. The porosity estimation results revealed a significant decrease (>75%) in the porosity of the coating after the sealing treatment. The electrochemical tests demonstrated that the sealed coating had a noble corrosion potential (–452 mV vs. Ag/AgCl), lower corrosion current density (3.07  $\mu\text{A}/\text{cm}^2$ ), and higher polarization resistance (162.649  $\text{k}\Omega \text{cm}^2$ ) relative to the as-sprayed coating, hence, was more corrosion resistant.

**Keywords:** WC–Co, corrosion, porosity, sealant, plasma spraying

**DOI:** 10.1134/S0031918X21110028

### INTRODUCTION

WC–Co coatings possess a combination of hardness and toughness due to the hard WC particles and ductile Co matrix [1]. These coatings have been applied to several metallic materials to increase their wear resistance, abrasion, and surface hardness. Thermal spraying processes such as air plasma spray (APS), high-velocity oxy-fuel (HVOF) spray, and detonation gun spray process are used to deposit these coatings [2, 3]. In thermal spraying processes, the material particles get heat from a heat source, and molten or semi-molten particles are generated and projected towards the surface of the substrate to form a thick coating. APS process provides high-temperature stability and improved interfacial bonding (30–70 MPa) to the coatings. However, the presence of cracks and a higher percentage of porosity (2–5%) in plasma spray coatings deteriorate their corrosion properties by allowing the corrosive media to proceed through the coating surface and reach the interface [4, 5].

Post-treatment methods such as re-melting, heat treatment, and sealing have been developed to reduce the microstructural defects in thermal spray coatings [6–8]. The re-melting and heat treatment processes can significantly improve the properties of the coat-

ings [9]. However, high thermal inputs during these processes can induce thermal stresses and eventually lead to producing cracks in the coatings [10]. The sealing process is a convenient and commonly used method to seal thermal spray coatings. In this process, the presence of certain discontinuities in the coatings such as pores and cracks allow the penetration of liquid sealants, and the subsequent heat treatment solidifies the sealants to seal the near-surface pores and cracks [11].

Sealant solutions require specific characteristics such as good wetting, low viscosity, and high surface tension to penetrate the porous structures [12]. Various sealant solutions have been used to seal the pores in thermal spray coatings to increase their corrosion properties. Wang et al. studied the effect of sodium orthosilicate, aluminum phosphate, and cerium salt sealants on the corrosion resistance of Fe-based coatings and found that the sealants effectively sealed the pores in the coatings and increased their corrosion resistance [13]. Shao et al. revealed that the sealing of plasma-sprayed  $\text{Cr}_2\text{O}_3$ – $\text{Al}_2\text{O}_3$  coatings by aluminum phosphate enhanced their corrosion performance [14]. Zhang et al. sealed HVOF sprayed nanostructured WC–CoCr cermet coatings with aluminum phosphate by ultrasonic excitation sealing technique.

Their study showed that the sealed coatings exhibited superior corrosion resistance in two different electrolytes [15].

Sol-gel sealant solutions have also received attention for the sealing processes because of their low viscosity. Amousoltani et al. investigated the use of sol-gel sealant solution containing the mixture of aluminum triisopropylate and 1,2-propanediol to seal HVOF sprayed WC-Co coatings. Their results revealed that the corrosion and wear properties of the coatings were improved after the sealing treatment [16]. Sealant solution consisting of aluminum isopropoxide  $\text{Al}(\text{OC}_3\text{H}_7)_3$  and isopropyl alcohol ( $\text{C}_3\text{H}_8\text{O}$ ) has been used to seal plasma sprayed YSZ coatings and HVOF sprayed WC-CoCr coatings, to improve their protective characteristics [17, 18]. Previous studies have proved that sol-gel precursors impregnate thermally sprayed coatings yielding a fine powder after in situ hydrolysis and condensation.

It is evident from the above literature review that the sealing treatment has been performed on various types of thermally sprayed coatings. However, the sealing can be more beneficial in plasma sprayed coatings because of their higher porosity and structural defects. It has been found that very few studies are conducted to improve the corrosion properties of plasma sprayed coatings by the sealing method. Moreover, no literature is available on the effect of sol-gel sealing treatment on the corrosion resistance of plasma-sprayed WC-12% Co coatings. Therefore, the purpose of this work was to seal the pores in plasma-sprayed WC-12% Co coating by the sol-gel sealant to improve its corrosion resistance. The coating was saturated by the sol-gel sealant solution followed by "curing" treatment. The microstructural features and the corrosion properties of the as-sprayed and sealed coatings were studied and compared.

## EXPERIMENTAL PROCEDURE

WC-12% Co powder with particle size 15–75  $\mu\text{m}$ , was sprayed onto AISI 321 stainless steel substrates ( $\varnothing = 25.4 \times 3 \text{ mm}$ ) using the air plasma spraying technique. Before the deposition, substrates were grit blasted (using Corundum of 60 mesh) at 0.7–0.8 MPa pressure and 5–10 mm standoff distance. After grit blasting, substrates were cleaned with acetone and ethanol, followed by drying in the oven. An average roughness ( $R_a$ ) of 4.6  $\mu\text{m}$  was achieved for a substrate. The WC-12% Co coatings were deposited on substrates with atmospheric plasma spray equipment (SX-80) using argon as a primary gas and hydrogen as a secondary gas.

Details of plasma spraying parameters are shown in Table 1.

The sealant was prepared by refluxing the mixture of optimized amounts of aluminum isopropoxide and isopropanol at 90°C for 4 h on a heating bath. The as-

**Table 1.** Plasma spraying parameters

Parameters	Quantity
Voltage	40 V
Current	650 A
Powder feed rate	50 g/min
Spray distance	120 mm
Primary gas (Ar) flow rate	30 L/min
Secondary gas ( $\text{H}_2$ ) flow rate	4 L/min

sprayed coatings were degreased by rinsing in acetone and ethanol, followed by drying in an oven. Then, the coating samples were immersed in the sealant solution for 10 min. The samples were then immersed in a 0.1 M HCl solution to catalyze gel formation, followed by curing at 120°C for 24 h to densify alumina gel. The sealed coating samples were slightly ground by a SiC paper (1200 grit) to remove the excess sealant from the coating surface to avoid any error in porosity calculations and electrochemical test results.

The porosity of as-sprayed and sealed coatings was measured by ASTM standard method (C20-00) to evaluate the effectiveness of sealing [19].

The following equations were used to calculate the porosity of the coatings.

$$\text{The volume of pores} = V = (M - S)/\rho_{\text{water}} \quad (1)$$

After the calculation of pore volume, porosity was determined using the following formula.

$$\text{Porosity (in \%)} = P = \frac{M - D}{V} \times 100. \quad (2)$$

Where  $M$  stands for saturated mass,  $D$  for dry mass, and  $S$  for wet mass in water,  $M$ ,  $D$ , and  $S$  are in grams;  $\rho$  is in  $\text{g}/\text{cm}^3$ ; and  $V$  is in  $\text{cm}^3$ .

The phase composition of the as-sprayed coating was studied by X-ray diffractometer (D8 Advance, Bruker, USA) with the diffraction angle ranged from 20° to 90°. The changes in morphology and microstructure of coatings before and after the sealing were inspected by a scanning electron microscope (SU8230, Hitachi, Japan), which operated at 20 kV. The presence of the sealant in the sealed coatings was confirmed by energy-dispersive X-ray spectroscopy (EDS). Corrosion properties of as-sprayed and sealed coatings were estimated by electrochemical tests in a 3.5 wt % NaCl solution at room temperature ( $35 \pm 1^\circ\text{C}$ ). The tests were conducted in a three-electrode cell coupled with a potentiostat (Interface 1000E, Gamry Instruments, USA) in which an Ag/AgCl (sat. KCl) was used as a reference electrode, graphite rod as an auxiliary electrode, and the coatings with 1  $\text{cm}^2$  exposed area as working electrodes. Before each test, the working electrode was immersed in the electrolyte for 1 hour to stabilize the potential. Open-circuit potential (OCP) was carried out for 1000 s, while potentiodynamic polarization (PD) plots were

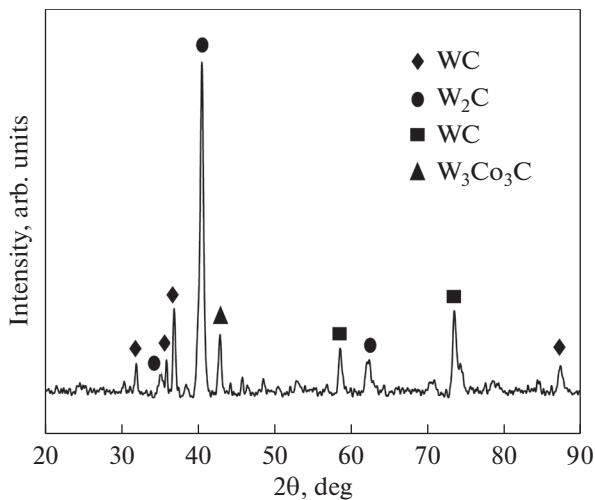


Fig. 1. XRD pattern of as-sprayed coating.

obtained by polarizing the surface of coating at a scan rate of 1 mV/s and a scan range of  $-0.5$  to  $-1.5$  V vs. OCP. Electrochemical impedance spectroscopy (EIS) curves of all the coating samples were attained in the frequency range of 100 kHz to 0.01 Hz with an ac pulsating potential of  $\pm 5$  mV. The Echem Analyst version 6.03 was used for kinetic parameters measurements and fitting of the Equivalent Electrical Circuit (EEC) model for the understanding of corrosion mechanism from PD and EIS curves, respectively.

## RESULTS AND DISCUSSION

Figure 1 presents the XRD pattern of the as-sprayed WC–12% Co coating, confirming the presence of WC,  $W_2C$ , W, and  $W_3Co_3C$  phases. The formation of the non-WC phases indicates significant oxidation and decarburization during the coating deposition. In the spraying process, the decarburization (loss of carbon) of WC particles occurs in the presence of high temperatures and oxygen by forming CO gas. The decarburization results in the formation of carbon deficient phases such as  $W_2C$  and W at the expense of WC [20].

Figure 2 illustrates the SEM micrographs of the plasma sprayed WC–12% Co coating before the sealing treatment. The coating microstructure represents the typical features of plasma sprayed coatings with certain defects. Moreover, the coating topography indicates a rough surface containing open and semi-closed pores. The porosity plays a critical role in determining the corrosion resistance of thermal spray coatings. The interconnected pores permit the electrolyte ions to penetrate and attack the substrate [21]. The presence of the porosity (diameter  $\leq 10$   $\mu\text{m}$ ) in the coatings is due to the entrapment of air or gases during the solidification process and the reaction of the depositing material particles with air [22]. The average

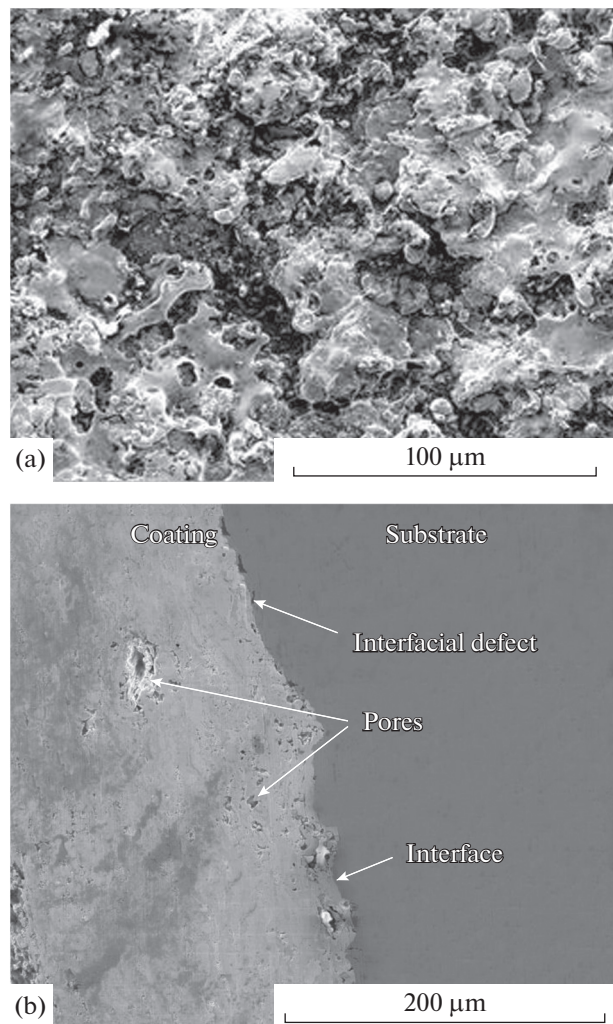


Fig. 2. SEM micrographs of as-sprayed coating (a) surface, (b) cross section.

porosity of as-sprayed coating measured by the ASTM standard C20-00 is found to be 3.51%. The deposited coating thickness is approximately  $220 \pm 10$   $\mu\text{m}$ , and the coating displays a good adhesion with the substrate, as is shown in (Fig. 2b) the cross-sectional micrograph.

Figure 3 shows the surface morphology of the sealed WC–12% Co coating. It seems that there are no apparent changes in the structure of coating after the sealing treatment. However, It can be seen from the image at higher magnification (Fig. 3b) that the sealant is present in the open pores of the sealed coating surface. It is evident from the micrographs that the pores aren't completely filled with the sealant particles after the sealing treatment. The main reason behind this phenomenon is that the sealant was in liquid form when it penetrated the pores, and the curing treatment caused excessive evaporation of the solvent. Consequently, the sealant decomposed by forming solid particles inside the pores [23]. The average porosity of

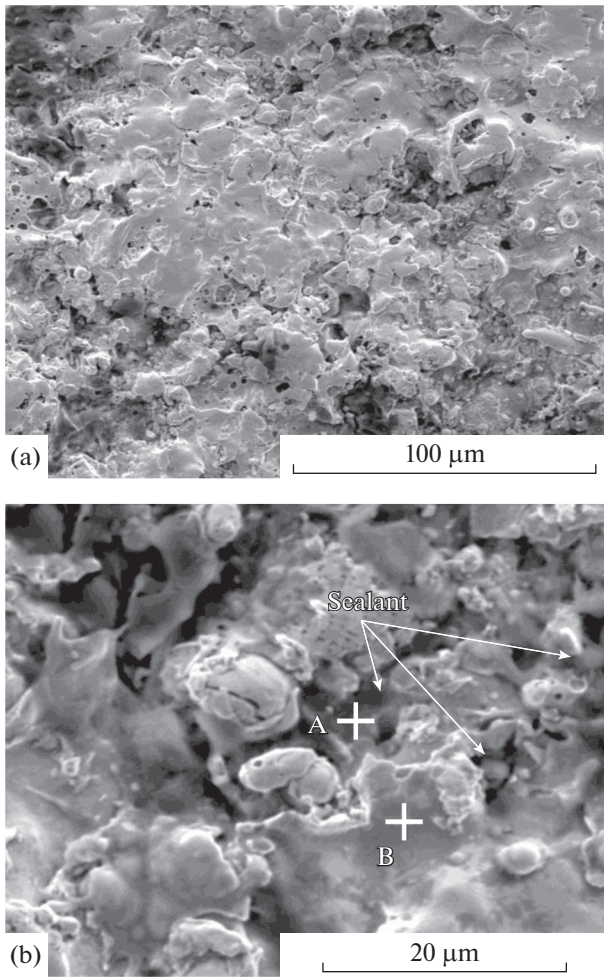


Fig. 3. SEM micrographs of sealed coating (a) 1500 $\times$ , (b) 6000 $\times$ .

sealed coating measured by the ASTM method C20-00 is 0.75%. The reduction in the porosity of the sealed coatings confirms the effectiveness of the sol-gel sealing method. It is expected that the reduced open porosity in the sealed coating will enhance its corrosion resistance.

The sealant particles in the pores of the sealed coating are also confirmed by the EDS analysis. The EDS point analysis of the porous areas (Point A) indicates the presence of Al (25.90 wt %) and O (36.16 wt %) along with primary elements of the coatings such as W, C, and Co. While in the dense area (Point B), only the primary elements including W (75.51 wt %), C (13.01 wt %), and Co (11.48 wt %) are present.

Figure 4 depicts the OCP curves of as-sprayed and sealed WC-12% Co coatings in 3.5 wt % NaCl solution for 1000 s immersion time. It can be seen that the potential values of both coatings remained steady throughout the test. At the end of the test, the OCP values of as-sprayed and sealed coatings are  $-539$  and  $-229$  mV vs. Ag/AgCl, respectively. The noble poten-

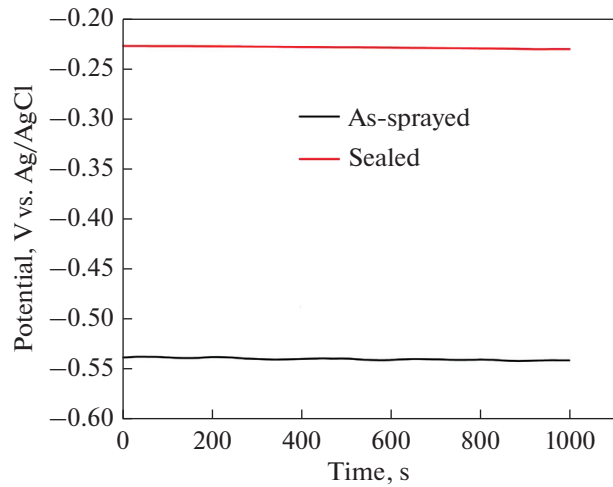
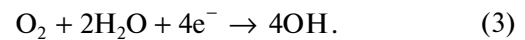


Fig. 4. OCP curves of as-sprayed and sealed coatings.

tial of the sealed coating is associated with its compact microstructure that hinders the penetration of electrolyte. This implies that pores inside the coating are sealed after the sealing treatment, and its open porosity is less than the as-sprayed coating due to which it has a better barrier effect [21].

Potentiodynamic polarization curves of as-sprayed and sealed coatings are shown in Fig. 5. The cathodic branch of the polarization curves is almost the same in both coatings. As the 3.5 wt % NaCl solution is neutral in nature, so the reduction during cathodic polarization on the coating surface will be an oxygen reduction reaction according to the following reaction in equation (3) [24].



The anodic branch of both coating samples shows the dissolution or activation region at a low potential, and resistance polarization region at high potential. The kinetic parameters such as corrosion potential ( $E_{\text{corr}}$ ), corrosion current density ( $I_{\text{corr}}$ ), and corrosion rate of as-sprayed and sealed coatings are calculated from polarization curves by Tafel fitting in the activation region of anodic and cathodic branches, and their values are illustrated in Table 2. According to polarization results, a positive shift in the  $E_{\text{corr}}$  values of the sealed coating ( $-452$  mV vs. Ag/AgCl) can be observed relative to the as-sprayed coating ( $-771$  mV

Table 2. Kinetic values of as-sprayed and sealed coatings in 3.5 wt % NaCl

Coating sample	$E_{\text{corr}}$ , mV	$I_{\text{corr}}$ , $\mu\text{A}/\text{cm}^2$	Corrosion rate, mpy
As-sprayed	$-771$	35.40	15.30
Sealed	$-452$	3.07	1.31

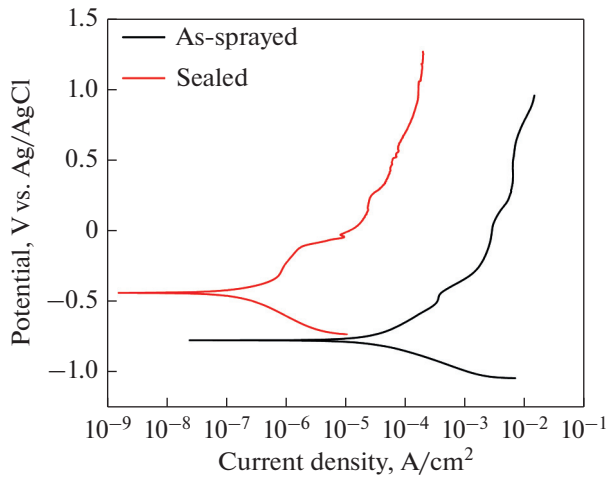


**Fig. 5.** Potentiodynamic polarization plots of as-sprayed and sealed coatings.

vs. Ag/AgCl). Generally, the  $E_{\text{corr}}$  describes the thermodynamic properties, and a higher value of the  $E_{\text{corr}}$  indicates low corrosion tendency [25]. It is obvious that the sealed coating has a higher  $E_{\text{corr}}$  value compared to the as-sprayed coating, which is clearly due to the pore sealing treatment that enhanced its barrier performance by making it less permeable to the electrolyte [26]. The lower  $E_{\text{corr}}$  value of the as-sprayed coating is associated with its relatively more porous and defective microstructure that provides the passage to the aggressive ions like  $\text{Cl}^-$  to penetrate through the coating.  $I_{\text{corr}}$  is an important parameter to evaluate the corrosion reaction kinetics, and a lower  $I_{\text{corr}}$  value indicates better corrosion resistance [27]. The  $I_{\text{corr}}$  values of as-sprayed and sealed coatings are 35.40 and 3.07  $\mu\text{A}/\text{cm}^2$ , respectively. Clearly, the  $I_{\text{corr}}$  value of the sealed coating is much lower than that of the as-sprayed coating, confirming the reduction in corro-

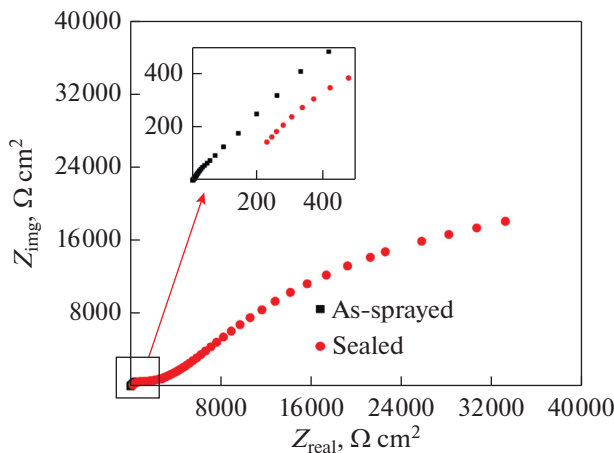


**Fig. 6.** Nyquist plots of as-sprayed and sealed coatings.

sion rate by more than ten times after the sealing treatment. From the results, it can be suggested the sealing treatment enhanced the compactness of the microstructure of the sealed coating and hence the corrosion resistance.

Figure 6 shows the impedance spectra (Nyquist plots) of as-sprayed and sealed coatings after immersion in 3.5 wt % NaCl. It can be seen that the capacitive arc of the sealed coating appears to be a semicircle, whereas that of as-sprayed coating is a flattened arc. This feature suggests that the characteristics of the protective films were different in respective coatings [15]. Besides, the Nyquist plot allows the comparisons of the capacitive arc of the coatings. It is a well-established fact that the larger radius of the capacitive arc represents higher corrosion resistance or charge transfer resistance due to the double layer [28]. It is evident from Fig. 6 that the sealed coating possesses higher corrosion resistance compared to the as-sprayed coating.

In order to calculate the quantitative parameters of the coating degradation mechanism, the impedance results presented in the Nyquist plots are fitted with the equivalent electrical circuit (EEC) model. The EEC models are shown in Fig. 7, and the derived values are illustrated in Table 3. In the EEC model,  $R_s$ ,  $R_p$ ,  $Y_c$ , and  $Y_d$  represents the solution resistance between the coating (working electrode) and the reference electrode, the polarization resistance offered by the coating, the non-ideal capacitive behavior of the coating/substrate interface, and the nonideal capacitive behavior of the dielectric material available in the coating, respectively. It can be seen that the  $R_p$  value of sealed coating (162.649  $\text{k}\Omega \text{ cm}^2$ ) is higher than that of as-sprayed (0.326  $\text{k}\Omega \text{ cm}^2$ ) coating. This means that the sealed coating has less porosity among all coatings, which is why it is the most corrosion-resistant [29]. The  $R_p$  value

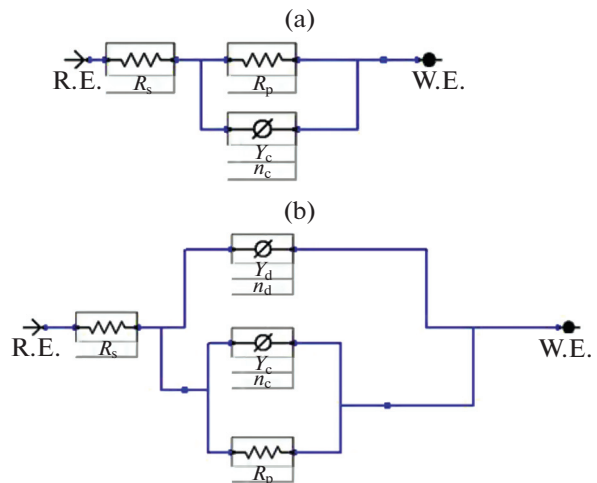


**Fig. 7.** Equivalent electrical circuit (EEC) model of (a) as-sprayed coating, (b) sealed coating.

**Table 3.** Impedance parameters of as-sprayed and sealed coatings obtained by EEC models fitting

Coated sample	$R_s, \Omega \text{ cm}^2$	$R_p, \text{k}\Omega \text{ cm}^2$	$Y_c, \text{S s}^n/\text{cm}^2$	$n_c$	$Y_d, \text{S s}^n/\text{cm}^2$	$n_d$
As-sprayed	5.375	0.326	$9.831 \times 10^{-3}$	0.595	—	—
Sealed	8.137	162.649	$6.843 \times 10^{-6}$	0.398	$3.764 \times 10^{-3}$	0.634

compliments the polarization result, as the sealed coating has a lower corrosion rate (1.31 mpy) compared to the as-sprayed coating. The  $R_s$  value is almost the same, because the solution remains the same for all the coating. All coatings show nonideal capacitive behavior because of the nonuniform surface morphology due to which the value of  $n$  lies between 0 and 1 ( $0 < n < 1$ ). The decrease in the  $Y_c$  indicates the good non-ideal capacitive layer on the interface of coating and the electrolyte. The EEC model of sealed coating is slightly different than that of the as-sprayed coating as is shown in Fig. 7b. The additional component  $Y_d$  is due to the dielectric sealing in the pores of as-sprayed coating, which makes its corrosion mechanism different from other coatings.

### CONCLUSIONS

Plasma sprayed WC–Co coating was sealed with the sol-gel sealant to increase its corrosion resistance. The porosity was significantly reduced from 3.51 to 0.75% after the sealing treatment. The electrochemical tests revealed that the corrosion barrier properties of the sealed coating were improved due to its lower porosity. The sealed coating exhibited a lower corrosion current, higher corrosion potential, and improved polarization resistance relative to the as-sprayed coating confirming its superior corrosion resistance.

### REFERENCES

- X. Liu, X. Song, H. Wang, X. Liu, F. Tang, and H. Lu, "Complexions in WC–Co cemented carbides," *Acta Mater.* **149**, 164–178 (2018).
- W. Tillmann, L. Hagen, D. Stangier, M. Paulus, M. Tolan, R. Sakrowski, D. Biermann, and D. Freiburg, "Microstructural characteristics of high-feed milled HVOF sprayed WC–Co coatings," *Surf. Coatings Technol.* **374**, 448–459 (2019).
- H. Myalska, L. Lusvarghi, G. Bolelli, P. Sassatelli, and G. Moskal, "Tribological behavior of WC–Co HVOF-sprayed composite coatings modified by nano-sized TiC addition," *Surf. Coatings Technol.* **371**, 401–416 (2019).
- L. Pawlowski, *The Science and Engineering of Thermal Spray Coatings: Second Edition* (2008).
- A. Y. Ivannikov, V. I. Kalita, D. I. Komlev, A. A. Radyuk, V. P. Bagmutov, I. N. Zakharov, and S. N. Parshev, "The effect of electromechanical treatment on structure and properties of plasma sprayed Ni–20Cr coating," *J. Alloys Compd.* **655**, 11–20 (2016).
- L. M. Zhang, S. D. Zhang, A. L. Ma, H. X. Hu, Y. G. Zheng, B. J. Yang, and J. Q. Wang, "Influence of sealing treatment on the corrosion behavior of HVOF sprayed Al-based amorphous/nanocrystalline coating," *Surf. Coatings Technol.* **353**, 263–273 (2018).
- K. M. Deen, M. Afzal, Y. Liu, A. Farooq, A. Ahmad, and E. Asselin, "Improved corrosion resistance of air plasma sprayed WC–12% Co cermet coating by laser re-melting process," *Mater. Lett.* **191**, 34–37 (2017).
- Z. B. Zheng, Y. G. Zheng, W. H. Sun, and J. Q. Wang, "Effect of heat treatment on the structure, cavitation erosion and erosion-corrosion behavior of Fe-based amorphous coatings," *Tribol. Int.* **90**, 393–403 (2015).
- Ciubotariu C.-R., Frunzäverde D., Mărginean G., Șerban V.-A., Bîrdeanu A.-V., "Optimization of the laser remelting process for HVOF-sprayed Stellite 6 wear resistant coatings," *Opt. Laser Technol.* **77**, 98–103 (2016).
- C. Batista, A. Portinha, R. M. Ribeiro, V. Teixeira, M. F. Costa, and C. R. Oliveira, "Morphological and microstructural characterization of laser-glazed plasma-sprayed thermal barrier coatings," *Surf. Coatings Technol.* **200**, 2929–2937 (2006).
- Q. Wang, C. S. Ramachandran, G. M. Smith, and S. Sampath, "Sliding wear behavior of air plasma sprayed  $\text{Al}_2\text{O}_3$  coatings sealed with aluminum phosphate," *Tribol. Int.* **116**, 431–439 (2017).
- G. M. Smith, M. Resnick, K. Flynn, G. Dwivedi, and S. Sampath, "Nature inspired, multi-functional, damage tolerant thermal spray coatings," *Surf. Coatings Technol.* **297**, 43–50 (2016).
- Y. Wang, S. L. Jiang, Y. G. Zheng, W. Ke, W. H. Sun, and J. Q. Wang, "Effect of porosity sealing treatments on the corrosion resistance of high-velocity oxy-fuel (HVOF)-sprayed Fe-based amorphous metallic coatings," *Surf. Coatings Technol.* **206**, 1307–1318 (2011).
- F. Shao, K. Yang, H. Zhao, C. Liu, L. Wang, and S. Tao, "Effects of inorganic sealant and brief heat treatments on corrosion behavior of plasma sprayed  $\text{Cr}_2\text{O}_3$ – $\text{Al}_2\text{O}_3$  composite ceramic coatings," *Surf. Coatings Technol.* **276**, 8–15 (2015).
- Y. Zhang, S. Hong, J. Lin, and Y. Zheng, "Influence of ultrasonic excitation sealing on the corrosion resistance of HVOF-sprayed nanostructured WC–CoCr coatings under different corrosive environments," *Coatings* **9**, 724–732 (2019).
- N. Amousoltani, H. Salimijazi, and M. Golzar, "Study of alumina sealing of HVOF thermally sprayed WC–Co coatings by sol-gel method," *Mater. Res. Express* **7**, 016410–016421 (2019).
- T. Troczynski, Q. Yang, and G. John, "Post-deposition treatment of zirconia thermal barrier coatings using sol-gel alumina," *J. Therm. Spray Technol.* **8**, 229–234 (1999).

18. S. Armada, B. G. Tilset, M. Pilz, R. Liltvedt, H. Bratland, and N. Espallargas, "Sealing HVOF thermally sprayed WC-CoCr coatings by sol-gel methods," *J. Therm. Spray Technol.* **20**, 918–926 (2011).
19. *ASTM C20-00, Standard Test Methods for Apparent Porosity, Water Absorption, Apparent Specific Gravity, and Bulk Density of Burned Refractory Brick and Shapes by Boiling Water* (Am. Soc. Test., 2015).
20. M. Jafari, M. H. Enayati, M. Salehi, S. M. Nahvi, and C. G. Park, "Comparison between oxidation kinetics of HVOF sprayed WC-12Co and WC-10Co-4Cr coatings," *Int. J. Refract. Met. Hard Mater.* **41**, 78–84 (2013).
21. E. Sadeghimeresht, N. Markocsan, and P. Nylén, "A comparative study of corrosion resistance for HVOF-sprayed Fe- and Co-based coatings," *Coatings* **6**, 26–28 (2016).
22. S. Zhou, X. Dai, and H. Zheng, "Microstructure and wear resistance of Fe-based WC coating by multi-track overlapping laser induction hybrid rapid cladding," *Opt. Laser Technol.* **44**, 190–197 (2012).
23. J. Kathikeyan, C. C. Berndt, A. Ristorucci, and H. Herman, "Ceramic impregnation of plasma sprayed thermal barrier coatings," in *Therm. Spray: Pract. Solut. Eng. Probl.*, Ed by C.C. Berndt. (ASM Int., 1996), pp. 477–482.
24. M. Pourbaix, *Atlas of Electrochemical Equilibria in Aqueous Solution* (NACE, 1974).
25. J. Chen, Y. Song, D. Shan, and E.-H. Han, "Modifications of the hydrotalcite film on AZ31 Mg alloy by phytic acid: The effects on morphology, composition and corrosion resistance," *Corros. Sci.* **74**, 130–138 (2013).
26. P. K. Aw, A. L. K. Tan, T. P. Tan, and J. Qiu, "Corrosion resistance of tungsten carbide based cermet coatings deposited by High Velocity Oxy-Fuel spray process," *Thin Solid Films* **516**, 5710–5715 (2008).
27. J.-H. Ding, H.-R. Zhao, Y. Zheng, X. Zhao, and H.-B. Yu, "A long-term anticorrosive coating through graphene passivation," *Carbon* **138**, 197–206 (2018).
28. Z. Xu, U. Eduok, and J. Szpunar, "Effect of annealing temperature on the corrosion resistance of MgO coatings on Mg alloy," *Surf. Coatings Technol.* **357**, 691–697 (2019).
29. S. Ammar, K. Ramesh, I. A. W. Ma, Z. Farah, B. Venugadaesvaran, S. Ramesh, and A. K. Arof, "Studies on SiO<sub>2</sub>-hybrid polymeric nanocomposite coatings with superior corrosion protection and hydrophobicity," *Surf. Coatings Technol.* **324**, 536–545 (2017).